

Broadband Optical Detection of Ferromagnetic Resonance From the Organic-Based Ferrimagnet V[TCNE]_x Using N-V Centers in Diamond

B.A. McCullian,^{1,*†} M. Chilcote,^{1,‡} V.P. Bhallamudi,² C.M. Purser,¹ E. Johnston-Halperin,¹ and P.C. Hammel^{1,§}

¹*Department of Physics, The Ohio State University, Columbus, Ohio 43210, USA*

²*Department of Physics, Indian Institute of Technology, Madras, Chennai 600 036, India*

(Received 3 December 2019; revised 9 April 2020; accepted 16 June 2020; published 13 August 2020)

Nitrogen-vacancy (N-V) center defects in diamond enable local, optical detection of magnons, owing to their sensitivity to gigahertz frequency magnetic field noise. Applied to ferromagnetic dynamics sensing, N-Vs can be used to sense an increase in the population of N-V-resonant magnons in a nearby ferromagnetic film, which arise from microwave drive of the uniform-mode ferromagnetic resonance and the subsequent scattering of uniform-mode magnon population throughout the magnon states. In this work we utilize N-V sensing to detect ferromagnetic resonance in films of the low magnetization, ferrimagnetic, coordination compound vanadium tetracyanoethylene (V[TCNE]_x). From an applications standpoint V[TCNE]_x has excellent magnetic resonance properties rivalling the best magnetic oxides and it can be deposited on a wide range of substrates, unlike most oxides. The remarkably low magnetization of V[TCNE]_x offers the chance to probe N-V-ferromagnet coupling in a yet-unexplored regime. We simultaneously detect broadband FMR spectroscopy of V[TCNE]_x films by both conventional microwave absorption and N-V techniques, finding few-gauss magnetic resonance linewidth and a magnetization of 49 G by both methods. Using spin-wave theory, we calculate the N-V-resonant spin-wave wavelengths to be on the order of tens of nanometers, with wavevectors on the order of 10⁸ m⁻¹. Our measurements highlight that the low magnetization of V[TCNE]_x results in very short wavelength spin waves at few-GHz frequencies, which can have significant advantage for future nanoscale magnonic applications.

DOI: 10.1103/PhysRevApplied.14.024033

I. INTRODUCTION

The use of magnons in insulating magnetic materials has attracted considerable attention for both fundamental research and applications ranging from microwave electronics, to spintronics, to quantum information [1–9]. In these roles, attractive properties include long spin lifetime and large-bandwidth tunability; further as insulators they are free of Ohmic losses. Traditionally, the inorganic magnetic insulator yttrium iron garnet (Y₃Fe₅O₁₂; YIG) has been the most attractive magnonic medium and has been widely adopted to investigate spin waves, microwave interactions, coupling to acoustic waves, and optical excitations [10–19]. However, high-quality YIG films have limitations. They can only be grown on lattice-matched substrates, such as gadolinium gallium garnet (Ga₃Gd₅O₁₂; GGG) [20], limiting integration with other common substrates, such as silicon. Moreover, YIG has

proven challenging to pattern using conventional fabrication techniques, raising barriers to on-chip integration. The microwave magnetic properties of the coordination compound vanadium tetracyanoethylene (V[TCNE]_x), on the other hand, make it a suitable candidate for many applications where YIG is limited [21]. High-quality-factor spin-wave resonances in thin films of V[TCNE]_x have been experimentally demonstrated in a functional microwave device [9]. Additionally, V[TCNE]_x is of significant interest for applications of cavity magnonics [22] and it has been shown to maintain high-quality-factor resonant linewidth when patterned at micron length scales [23]. These results position V[TCNE]_x as a promising alternative to YIG for emerging applications in on-chip magnonics. Realizing this potential, however, requires a detailed understanding of the local behavior of spin-wave excitations in magnonic microstructures and integrated circuits.

A central challenge to developing this understanding is characterizing the magnetic relaxation processes. In ferromagnetic resonance the uniform-mode precession of spins is driven by a microwave frequency magnetic field. The uniform mode relaxes to available thermal reservoirs: phonons, magnons, and conduction electrons.

*mccullian.1@buckeyemail.osu.edu

†hammel@physics.osu.edu

‡These authors contributed equally to this work.

Conventional microwave-absorption-based FMR techniques measure this relaxation through the FMR linewidth, which has contributions from all of these relaxation channels [24]. Inelastic light-scattering techniques like Brillouin light scattering (BLS) can directly probe magnons, which result from scattering processes, but are unable to probe magnons of very short wavelength, in addition to being diffraction limited [18]. The nitrogen-vacancy defect (N-V center) in diamond has emerged as a unique probe of ferromagnetic dynamics owing to its pointlike nature and its spin-dependent PL, which renders the N-V sensitive to local, gigahertz frequency, magnetic fields. N-V detection of ferromagnetic resonance relies both on the coupling of the uniform FMR mode to the incoherent magnon bath and the coupling of the N-V-resonant magnons to nearby N-V spins [25–30]. N-V detection of ferromagnetic resonance provides valuable insight to microwave-driven spin-chemical potential [25], magnetoacoustic coupling [26], spin-wave transport [31,32], damping in ferromagnets [27], and spatially resolved studies of spin-wave modes in patterned disks [28].

A yet unexplored regime of N-V-ferromagnet coupling is in extremely low magnetization materials like V[TCNE]_x. In this work we use ensembles of N-V centers to optically detect ferromagnetic resonance at room temperature in films of V[TCNE]_x. We simultaneously detect broadband FMR using both N-V and conventional microwave-absorption techniques, verifying that the N-V relaxation signal is a result of the driven FMR. Despite having more than an order of magnitude smaller magnetization than ferromagnetic materials previously studied with N-Vs [25,27–29], meaning that the stray magnetic fields produced by the V[TCNE]_x is consequently smaller, we find that N-V–V[TCNE]_x coupling is readily detectable using our simple N-V scheme. N-V-detected FMR spectroscopy shows excellent spectral agreement with the conventional FMR allowing us to extract the effective magnetization and gyromagnetic ratio of the V[TCNE]_x using both methods. For modest input microwave power, we observe a sharp N-V-detected FMR line. Relying on spin-wave theory, we calculate the length scale of the N-V-resonant spin waves to be on the order of tens of nm, extending well into the exchange branch of the spin waves, a regime beyond the range of techniques like BLS.

II. EXPERIMENTAL SETUP

We use two samples of V[TCNE]_x on diamond. Sample N-V–P uses a polycrystalline diamond substrate and sample N-V–S uses a single-crystal diamond. The single-crystal diamond we use in N-V–S has (100)-oriented faces. Both diamonds have native nitrogen impurity concentrations of less than 1 parts per million. Each diamond is irradiated with nitrogen to a peak concentration of 200

parts per million nitrogen (the peak implantation depth for the polycrystalline diamond is 50 nm, and is 25 nm for the single-crystal diamond, according to SRIM calculations [33]). After irradiation, the diamonds are annealed at 850 °C for 2 h at 100 mTorr in a 4% hydrogen-in-argon environment to promote N-V center formation. The concentration of N-V centers is a few parts per million after annealing. V[TCNE]_x is deposited onto the surface of a diamond substrate containing N-V centers via low temperature (60 °C) chemical vapor deposition in an argon environment inside a glovebox [34]. The V[TCNE]_x is deposited during two different growths, to thicknesses of 150 nm on sample N-V–P and 1.5 μm on sample N-V–S. To confirm the quality of the V[TCNE]_x growth, the single-crystal sample N-V–S is sealed in a sample tube for measurement in a cavity FMR setup. The cavity FMR signal in Fig. 1 shows a full width at half maximum of 2.05 ± 0.01 G (peak-to-peak linewidth 1.18 ± 0.01 G) at 9.61 GHz indicating excellent magnetic resonance quality [9]. A confirmation sample of 1.5-μm-thick V[TCNE]_x simultaneously deposited on sapphire also shows excellent resonance properties, indicating that V[TCNE]_x deposits well on diamond. Both N-V–P and N-V–S are ultimately sandwiched onto a microstrip antenna (5 nm Ti/285 nm Ag/10 nm Au), which is lithographically patterned on a sapphire substrate to a taper 15 μm wide at the narrowest. Epoxy is used to protect the V[TCNE]_x from oxidation [35]. The final sample geometry and an optical micrograph of sample N-V–S is shown in Fig. 1.

We simultaneously detect FMR of V[TCNE]_x using N-V fluorescence and conventional microwave absorption. Microwaves 100% amplitude modulated at $f_{\text{mod}} \sim 1.2$ kHz are sent from a microwave generator (Wiltron 68147B) through the microstrip in a transmission geometry. Microwave transmission is measured with a microwave diode (Krytar 303BK) using a lock-in amplifier (Signal Recovery 7265) referenced to f_{mod} . A 532-nm green laser (LaserGlow L532001FX) is focused onto the N-V ensemble by a microscope objective (Mitutoyo M Plan Apo 20). We probe all N-V orientations in our experiments. The green laser optically pumps the N-Vs into a maximally fluorescent spin-0 state. The laser power for all measurements is 300 mW and is defocused to a beam approximately 10 μm in diameter, centered on the microwave antenna. Additional measurements are taken as a function of position both along and moving perpendicularly away from the antenna and are qualitatively similar. N-V fluorescence is collected through the same objective, filtered from the green pump beam by a dichroic mirror and red long-pass filtering, and is recorded by a photodiode (Thorlabs DET110), amplified by a current-to-voltage preamplifier (RHK IVP300), and fed into a second lock-in amplifier. Both the dc PL of the N-Vs and the changes of N-V PL at f_{mod} are recorded. The in-plane magnetic field is swept while microwaves are applied at fixed frequency. The

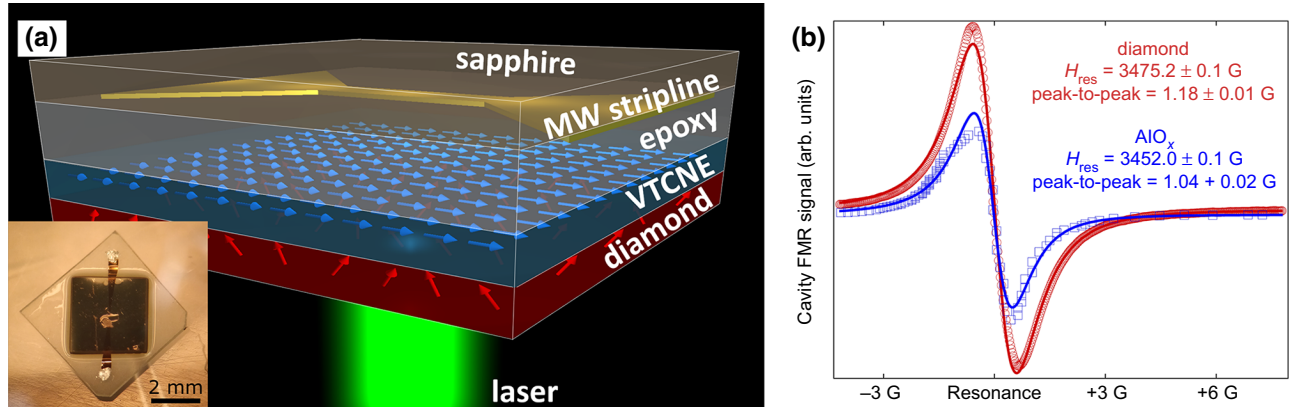


FIG. 1. Sample schematic and cavity FMR. (a) $\text{V}[\text{TCNE}]_x$ film is deposited on the surface of the diamond substrate, which contains an implanted layer of N-V centers tens of nanometers below the surface. Microstrip patterned on sapphire substrate is flipped onto a $\text{V}[\text{TCNE}]_x$ -diamond stack and encapsulated with optical grade epoxy. (Inset) Optical micrograph of the single-crystal-diamond sample. $\text{V}[\text{TCNE}]_x$ forms a black film on the surface of the diamond (oriented square). Gold colored microstrip is visible as patterned on sapphire substrate (clear, diagonal). (b) 9.61-GHz cavity FMR signal of $\text{V}[\text{TCNE}]_x$ film, which is simultaneously deposited on single-crystal diamond (sample N-V-S) and on sapphire. Signals are shifted in magnetic field in order to compare linewidths. Peak-to-peak linewidths are $1.18 \pm 0.01 \text{ G}$ (grown on diamond) and $1.04 \pm 0.02 \text{ G}$ (grown on sapphire). Solid lines are fits to Eq. (1).

phase of the N-V lock-in is set by driving the N-V centers with 2.87-GHz microwaves at zero magnetic field, such that a reduction of N-V PL results in a positive in-phase N-V lock-in signal. We typically see a 6–8 % decrease in our ensemble N-V PL when we excite the N-V ground state at zero applied magnetic field with approximately 50 mW microwave power.

III. EXPERIMENTAL RESULTS

In Fig. 2 we plot the N-V and microwave-absorption-detected FMR of sample N-V-P at 1 GHz for a microwave power of $100 \mu\text{W}$ using a lock-in time constant of 300 ms. The N-V and microwave absorption signals in Fig. 2 are averaged 20 times. The N-V signal is displayed as a percent change in N-V PL by taking the lock-in-detected changes of N-V PL at f_{mod} and dividing by the dc PL. We see that there is a change in N-V PL at a static field of about 290 G. The microwave transmission has a dip at about the same magnetic field. This microwave absorption is a direct measure of the $\text{V}[\text{TCNE}]_x$ FMR and confirms that the N-V PL change is in response to driven FMR. We fit each signal to a Lorentzian response [36] that includes both an absorptive and dispersive term:

$$f(H) = A_0 + A_1 H + [A_{\text{abs}} + A_{\text{disp}}(H - H_{\text{res}})] / \left[(H - H_{\text{res}})^2 + \left(\frac{\Delta H}{2} \right)^2 \right]. \quad (1)$$

Here H is the applied magnetic field, A_0 is a constant offset, A_1 is a linear background, A_{abs} and A_{disp} are scaling

coefficients for the absorptive and dispersive parts of the response, H_{res} is the resonance field, and ΔH is the full width at half maximum linewidth. The A_0 and A_1 are set to zero for the N-V signal fit. From the fitting we extract a full width at half maximum linewidth of $2.31 \pm 0.25 \text{ G}$ from the N-V detection and $3.87 \pm 0.07 \text{ G}$ from microwave absorption.

The N-V fluorescence response to driven FMR can be understood in terms of the FMR relaxation process [25]. When microwaves excite uniform-mode FMR (the $\vec{k} = 0$ magnon mode), the driven uniform mode undergoes scattering with both the phonon bath and the magnon bath that relaxes it to thermal equilibrium. In particular, the four-magnon-scattering process takes a uniform-mode magnon and scatters it off a thermally occupied $\vec{k} \neq 0$ magnon. The product of this scattering is two outgoing $\vec{k} \neq 0$ magnons. Some of these four-magnon-scattering events result in magnons having frequencies matched to the N-V spin transitions. These N-V-resonant magnons produce dipole magnetic fields, which extend outside the $\text{V}[\text{TCNE}]_x$ layer, and which couple to and thus relax the optically polarized spin of nearby N-V centers. The N-V senses the increase of N-V-resonant magnons as noise, since the magnon-scattering process is incoherent and results in increased incoherent magnetic field noise at the N-V frequency. This noise increases the relaxation rate of the $\text{N-V} |m_s = 0\rangle$ spin state. When the N-Vs are illuminated with green laser, the amplitude of the N-V ensemble fluorescence depends on the rates of all allowed N-V transitions. Thus, the change of N-V relaxation rate arising from driven FMR manifests as a reduction of the N-V PL. We measure the linewidth of the N-Vs in sample N-V-P to be 3.6 G at $10 \mu\text{W}$ microwave

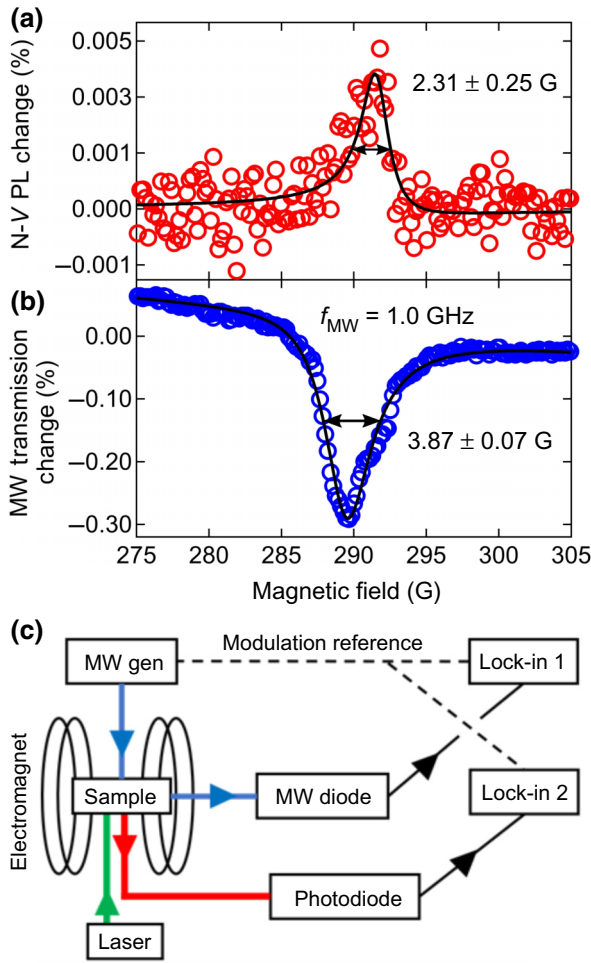


FIG. 2. N-V and microwave-absorption-detected FMR of $\text{V}[\text{TCNE}]_x$ on polycrystalline diamond. (a) N-V-detected FMR signal from sample N-V-P with microwaves applied at 1 GHz and 100 μW input microwave power. N-V signal reported as percent change by taking the lock-in detected N-V signal and dividing by the dc PL. (b) Simultaneously detected microwave-absorption FMR signal from the $\text{V}[\text{TCNE}]_x$ we use to verify that N-V PL changes result from driven FMR. N-V and microwave-absorption signals are fit to Eq. (1) to extract the FMR linewidth. (c) Experimental schematic. 100% amplitude modulated ($f_{\text{mod}} \sim 1.2$ kHz) microwaves are sent from the microwave generator through the microstrip in transmission to drive FMR. Magnetic field is swept in plane using an electromagnet. Microwave transmission is detected using a microwave diode and measured at f_{mod} using a lock-in amplifier. Continuous green laser excites the N-V spin ensemble, red N-V PL is collected and measured using a photodiode. Both the dc PL and the PL changes at f_{mod} are recorded.

power. The N-V-detected FMR linewidth is sensitive to this N-V linewidth only insofar as the N-V linewidth determines which magnons are relaxing the N-V. The FMR linewidth detected by the N-V is primarily set by the range of microwave frequencies that excite uniform-mode FMR of the ferromagnetic layer, since it is the excitation

of the FMR that gives rise to an elevated population of N-V-resonant magnons, and ultimately the N-V relaxation signal.

Both the N-V and microwave-absorption-detected FMR linewidths of sample N-V-P in Fig. 2 are broader than the cavity FMR detected for sample N-V-S. A potential discrepancy between the conventional FMR schemes may arise from the detection; cavity FMR has a homogeneous microwave excitation and can result in a sharper measured linewidth compared to microstrip excitation, which is spatially inhomogeneous. Another possibility is that the microwave drive fields near the microstrip are larger than those used in the cavity FMR measurement, which can result in a nonlinear FMR response, which is known to broaden the FMR line [24]. The N-V response depends on both the linewidth of the FMR [27] and the magnon scattering meaning that the N-V-detected line shape can be quite different from the conventional FMR line shape. The appearance of the N-V and microwave-absorption-detected FMR peaks at nearly identical fields suggests that there is no significant temperature increase at the laser spot, despite the 300-mW laser excitation power.

In Fig. 3 we use N-V detection and microwave absorption to perform FMR spectroscopy of the sample N-V-S. The magnetic field is applied in the plane of the $\text{V}[\text{TCNE}]_x$ film and makes an angle of about 54° with respect to all four N-V bond directions. This results overall in two N-V states, one of mixed $|m_s = 0\rangle$ and $|m_s = -1\rangle$ characteristic and one of mixed $|m_s = 0\rangle$ and $|m_s = +1\rangle$ characteristic. The magnetic field strength is swept for varying microwave frequencies at an input microwave power of 10 mW. The microwave power we use is increased compared to Fig. 2 in order to achieve high SNR N-V signals while avoiding the need to average multiple field sweeps. These data are single-sweep responses using a 300-ms lock-in time constant. The microwave transmission curves here have a linear background removed. As before we see that the FMR dip in microwave transmission is accompanied by a change in N-V PL. Though the microwave-absorption signal is increasing with increasing frequency, the N-Vs experience increasing off-axis magnetic field with increasing resonance frequency. Off-axis magnetic fields decrease N-V PL and the spin contrast of N-V PL [37], hence the N-V-detected FMR signal diminishes with increasing uniform-mode FMR frequency. At each frequency we fit with Eq. (1) and extract the resonance field. We use these resonance fields to plot and fit the FMR dispersion of the $\text{V}[\text{TCNE}]_x$ using each technique. Fits are to the uniform-mode response of a magnetic thin film with magnetic field applied in plane [38]:

$$H_{\text{res}}(f_{\text{MW}}) = \sqrt{\left(\frac{2\pi f_{\text{MW}}}{\gamma}\right)^2 + (2\pi M_{\text{eff}})^2} - 2\pi M_{\text{eff}}. \quad (2)$$

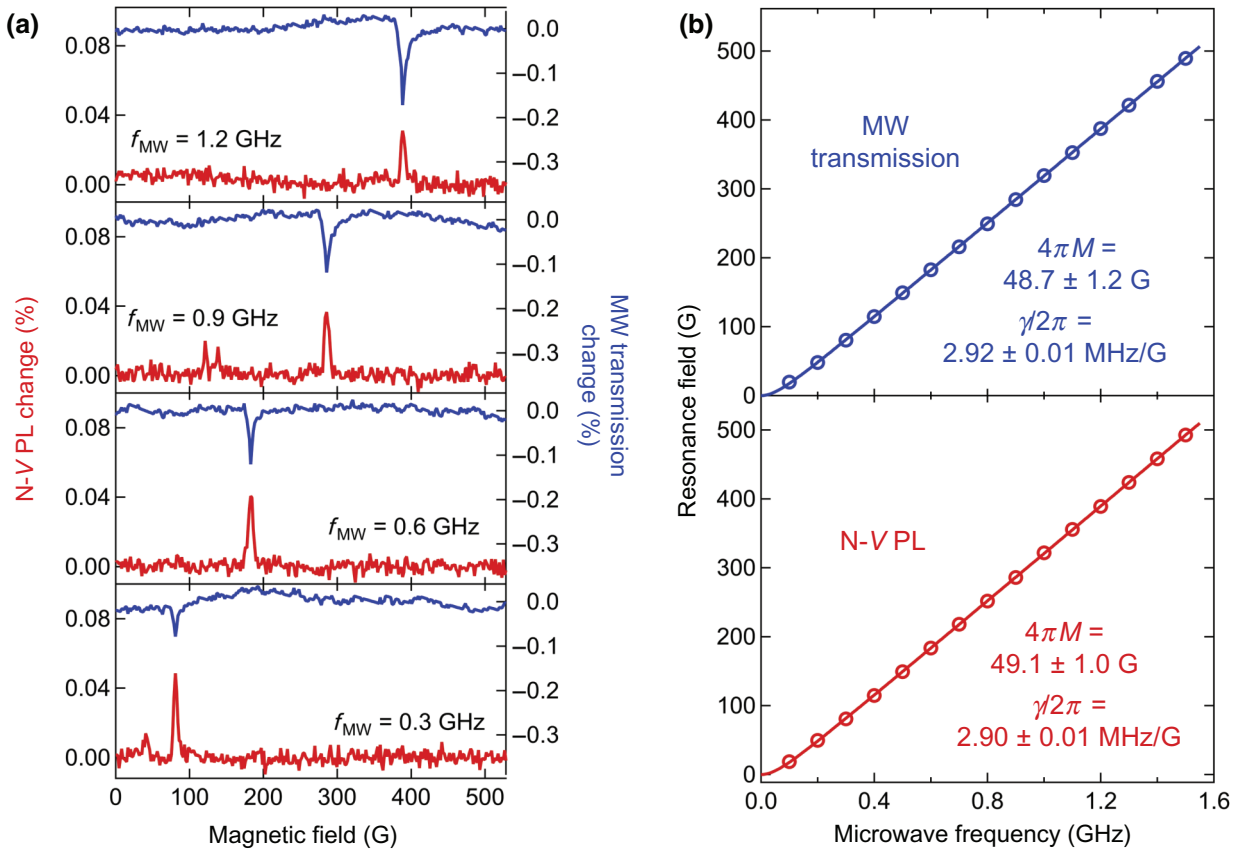


FIG. 3. Broadband N-V and microwave absorption $V[\text{TCNE}]_x$ FMR signals and FMR dispersion. (a) N-V and microwave-absorption-detected $V[\text{TCNE}]_x$ FMR signals of sample N-V-S for four distinct microwave frequencies at +10 dBm input microwave power. (b) Fitted resonance field versus microwave frequency for both microwave absorption and N-V-detected FMR. Fits to Eq. (2) are used to extract the $V[\text{TCNE}]_x$ effective magnetization and gyromagnetic ratio. The extracted parameters using the two techniques are in excellent agreement.

Here H_{res} is the static magnetic field on resonance, f_{MW} is the microwave frequency, $\gamma/2\pi$ is the gyromagnetic ratio, and $4\pi M_{\text{eff}}$ is the effective magnetization of the film. Fitting the FMR dispersions to Eq. (2) we find that microwave absorption and N-V PL measure the effective magnetization of the $V[\text{TCNE}]_x$ to be $48.7 \pm 1.2 \text{ G}$ and $49.1 \pm 1.0 \text{ G}$, respectively. These values differ somewhat from the literature but are in close agreement with one another [39]. We also find gyromagnetic ratios of $2.92 \pm 0.01 \text{ MHz/G}$ (microwave absorption) and $2.90 \pm 0.01 \text{ MHz/G}$ (N-V), which are in good agreement with one another and the literature.

IV. DISCUSSION

We can determine the wavelength of the N-V-resonant spin waves probed in our experiment by calculating the spin-wave dispersion. The dispersion relation is

$$\begin{aligned} (\omega_k/\gamma)^2 &= (\omega_{\text{FMR}}/\gamma + 4\pi M \lambda_{\text{ex}} k^2) \\ &\times (\omega_{\text{FMR}}/\gamma + 4\pi M \lambda_{\text{ex}} k^2 + 4\pi M \sin^2 \theta_k), \end{aligned} \quad (3)$$

where ω_k is the frequency of the magnon with wavevector k , ω_{FMR} is the frequency of the uniform-mode FMR, λ_{ex} is the exchange constant in $V[\text{TCNE}]_x$, and θ_k is the angle of the spin-wave propagation direction relative to the magnetization [24]. We consider as an example the condition when the uniform-mode FMR frequency is 1 GHz, which occurs at a magnetic field of 290 G. The ground-state Hamiltonian of an N-V center including the Zeeman interaction with the magnetic field is $\mathcal{H} = DS_z^2 + \gamma \vec{B} \cdot \vec{S}$ where D is the ground-state N-V splitting of 2.87 GHz, γ is the N-V gyromagnetic ratio of 2.8 MHz/G, and S_i are the spin-1 Pauli matrices. The angle between the N-V axis and the static magnetic field is 54° for all N-V orientations. At 290 G we calculate that the two N-V frequencies are 2.7 and 3.7 GHz. Then, using the measured $4\pi M$ and the literature [9] value of $\lambda_{\text{ex}} = 4.61 \times 10^{-16} \text{ m}^2$ and noting that the stray field produced by a spin wave is largest when the spin wave propagates with $\theta_k = 90^\circ$ [40], we calculate the wavevector and wavelength of the N-V-resonant spin waves. We find that the spin wave resonant with the mixed $|m_s = 0\rangle$ and $|m_s = +1\rangle$ characteristic N-V branch has $k = 2.1 \times 10^8 \text{ m}^{-1}$ and $\lambda = 30 \text{ nm}$ and that the spin wave

resonant with the mixed $|m_s = 0\rangle$ and $|m_s = -1\rangle$ characteristic N-V branch has $k = 1.7 \times 10^8 \text{ m}^{-1}$ and $\lambda = 37 \text{ nm}$. These spin-wave wavevectors are well into the exchange branch of the spin-wave dispersion and are even larger than those recently reported by Lee-Wong *et al.* [41], where the authors highlight the potential for N-V sensitivity to spin-wave wavevectors into the 10^8 m^{-1} . The physical interpretation of these very large N-V-detected wavevectors and short spin-wave wavelengths is that in V[TCNE]_x the spin-wave wavelength must be very short in order for the spin wave to be at considerably higher frequency than the uniform-mode FMR, which is set by the exchange contribution to the spin-wave frequency $4\pi M \lambda_{\text{ex}} k^2$ in Eq. (3). Despite the exchange constant λ_{ex} of V[TCNE]_x and YIG being similar [9], the appearance of the saturation magnetization in the exchange contribution to the spin-wave frequency means that the N-V-resonant wavelengths in V[TCNE]_x are about an order of magnitude shorter than those in YIG due to the difference in saturation magnetization.

It is useful to compare the strength of the N-VPL signal with our previous investigations of YIG using the same N-V detection protocol and sample geometry. YIG films like those studied by our group typically have a 10 GHz cavity-FMR linewidth of 6–8 G [30]. Despite the sharper V[TCNE]_x line we find that the fractional change in N-V PL from V[TCNE] FMR is smaller than the change in N-V PL from YIG FMR by more than an order of magnitude for comparable input microwave power. This can be understood as arising from the reduced magnetization of V[TCNE]_x, both directly and indirectly from the consequent reduction of the wavelength of the probed magnons. The effective magnetization of YIG [42] is about 1800 G—about 37 times higher than that of the V[TCNE]_x studied here. The strength of the dipole fields created by a sheet of magnons scales linearly with this magnetization [25], directly reducing the N-V signal. The second contribution to the N-V signal amplitude can be understood from the spatial transfer function of dynamic magnetic fields from the film to the N-Vs. The dipole magnetic fields from the magnons scale as $k^2 e^{-2kd}$ where k is the magnon wavevector and d is the N-V-film separation [28]. Only magnons separated from the N-V layer by a few multiples of the N-V-resonant spin-wave wavelength efficiently couple to the N-Vs. We do not see an appreciable increase in the N-V-detected FMR signal amplitude in sample N-V-S, despite increasing the thickness of the V[TCNE]_x layer by a factor of 10 as compared to sample N-V-P, which we attribute to the very short (tens of nm) wavelength magnons, which are responsible for N-V relaxation. In N-V experiments probing YIG, the N-V-resonant magnon length scales are an order of magnitude larger, thus more of the thickness of the YIG film can contribute to N-V relaxation.

The volume of V[TCNE]_x probed by the N-V and microwave-absorption techniques is quite different.

Microwaves from the microstrip antenna excite and detect an area of the V[TCNE]_x film approximately set by the area of the microstrip antenna (about $100 \mu\text{m} \times 5 \text{ mm}$). Since the N-Vs are sensing magnons on the tens of nm length scale, the area of V[TCNE]_x sensed by the N-Vs is set primarily by the laser spot, which in this experiment is about $10 \mu\text{m}$ in diameter. Comparing the area of V[TCNE]_x probed by the two techniques, we find that the N-V signal comes from a V[TCNE]_x sample area about 10^4 times smaller than the microwave-absorption signal.

V. CONCLUSION

In this work we demonstrate optical, broadband detection of ferromagnetic resonance in the organic-based ferrimagnet V[TCNE]_x using an ensemble of N-V centers. We find that despite the low magnetization of V[TCNE]_x, the FMR is readily detectable using N-V relaxometry. N-V-detected FMR spectroscopy agrees well with simultaneous microwave-absorption measurements allowing for determination of the effective magnetization and gyromagnetic ratio both locally and globally. We find that the N-V-resonant magnons responsible for the optical detection have a wavelength scale of tens of nm and wavevectors on the order of 10^8 m^{-1} , demonstrating the sensitivity of the N-Vs to these short wavelength magnons. Our work highlights the importance of studying magnetic materials with low saturation magnetization, which in V[TCNE]_x results in very short wavelength spin waves at few-GHz frequencies, a promising feature for nanoscale magnonic applications.

Continuation of this work should include time-resolved N-V detection of V[TCNE]_x FMR. Direct measurement of the N-V spin lifetime may provide enhanced signal to noise, and could be a means to measure magnon-scattering rates. Careful alignment of the static magnetic field to the N-V axis, potentially in single-N-V measurements, could enable N-V–V[TCNE]_x coupling measurements at frequencies in excess of 10 GHz because of the low V[TCNE]_x magnetization. This allows for direct quantitative comparison of the sensitivity of cavity FMR with the N-V relaxometry technique. Finally, engineering nonzero wavevector spin-wave modes in V[TCNE]_x may provide a means of coherently coupling N-Vs and spin waves in V[TCNE]_x for further comparison with YIG [31,32].

ACKNOWLEDGMENTS

This work is primarily supported by the Center for Emergent Materials at the Ohio State University, a National Science Foundation (NSF) MRSEC through award number DMR-2011876 (FMR and N-V measurements). Support for V[TCNE]_x growth is provided by NSF EFMA-1741666 and DMR-1507775. We acknowledge use

of Ohio State University Nanosystems Laboratory shared facilities (NSF DMR-2011876).

-
- [1] L. Trifunovic, F. L. Pedrocchi, and D. Loss, Long-Distance Entanglement of Spin Qubits via Ferromagnet, *Phys. Rev. X* **3**, 041023 (2013).
 - [2] M. Wu, B. A. Kalinikos, L. D. Carr, and C. E. Patton, Observation of Spin-Wave Soliton Fractals in Magnetic Film Active Feedback Rings, *Phys. Rev. Lett.* **96**, 187202 (2006).
 - [3] A. A. Serga, A. V. Chumak, B. Hillebrands, and Y. I. G. magnonics. *J. Phys. D: Appl. Phys.* **43**, 264002 (2010).
 - [4] B. A. Kalinikos, M. M. Scott, and C. E. Patton, Self-Generation of Fundamental Dark Solitons in Magnetic Films, *Phys. Rev. Lett.* **84**, 4697 (2000).
 - [5] Y. S. Gui, Y. Xiao, L. H. Bai, S. Hemour, Y. P. Zhao, D. Houssameddine, K. Wu, H. Guo, and C. M. Hu, High sensitivity microwave detection using a magnetic tunnel junction in the absence of an external applied magnetic field, *Appl. Phys. Lett.* **106**, 152403 (2015).
 - [6] Y. S. Gui, N. Mecking, and C. M. Hu, Quantized Spin Excitations in a Ferromagnetic Microstrip From Microwave Photovoltage Measurements, *Phys. Rev. Lett.* **98**, 217603 (2007).
 - [7] T. Giamarchi, C. Rüegg, and O. Tchernyshyov, Bose-Einstein condensation in magnetic insulators, *Nat. Phys.* **4**, 198 (2008).
 - [8] A. V. Chumak, A. A. Serga, and B. Hillebrands, Magnon transistor for all-magnon data processing, *Nat. Commun.* **5**, 4700 (2014).
 - [9] N. Zhu, X. Zhang, I. H. Froning, M. E. Flatté, E. Johnston-Halperin, and H. X. Tang, Low loss spin wave resonances in organic-based ferrimagnet vanadium tetracyanoethylene thin films, *Appl. Phys. Lett.* **109**, 082402 (2016).
 - [10] X. Zhang, C.-L. Zou, L. Jiang, and H. X. Tang, Strongly Coupled Magnons and Cavity Microwave Photons, *Phys. Rev. Lett.* **113**, 156401 (2014).
 - [11] Y. Tabuchi, S. Ishino, A. Noguchi, T. Ishikawa, R. Yamazaki, K. Usami, and Y. Nakamura, Coherent coupling between a ferromagnetic magnon and a superconducting qubit, *Science* **349**, 405 (2015).
 - [12] Y. R. Shen and N. Bloembergen, Interaction between light waves and spin waves, *Phys. Rev.* **143**, 372 (1966).
 - [13] A. Osada, R. Hisatomi, A. Noguchi, Y. Tabuchi, R. Yamazaki, K. Usami, M. Sadgrove, R. Yalla, M. Nomura, and Y. Nakamura, Cavity Optomagnonics with Spin-Orbit Coupled Photons, *Phys. Rev. Lett.* **116**, 223601 (2016).
 - [14] C. Kittel, Excitation of spin waves in a ferromagnet by a uniform rf field, *Phys. Rev.* **110**, 1295 (1958).
 - [15] C. Kittel, Interaction of spin waves and ultrasonic waves in ferromagnetic crystals, *Phys. Rev.* **110**, 836 (1958).
 - [16] J. A. Haigh, S. Langenfeld, N. J. Lambert, J. J. Baumberg, A. J. Ramsay, A. Nunnenkamp, and A. J. Ferguson, Magneto-optical coupling in whispering-gallery-mode resonators, *Phys. Rev. A* **92**, 063845 (2015).
 - [17] M. Goryachev, W. G. Farr, D. L. Creedon, Y. Fan, M. Kostylev, and M. E. Tobar, High-Cooperativity Cavity QED with Magnons at Microwave Frequencies, *Phys. Rev. Appl.* **2**, 054002 (2014).
 - [18] S. O. Demokritov, B. Hillebrands, and A. N. Slavin, Brillouin light scattering studies of confined spin waves: Linear and nonlinear confinement, *Phys. Rep.* **348**, 441 (2001).
 - [19] L. Bai, M. Harder, Y. P. Chen, X. Fan, J. Q. Xiao, and C. M. Hu, Spin Pumping in Electrodynamically Coupled Magnon-Photon Systems, *Phys. Rev. Lett.* **114**, 227201 (2015).
 - [20] Y. Sun, Y.-Y. Song, and M. Wu, Growth and ferromagnetic resonance of yttrium iron garnet thin films on metals, *Appl. Phys. Lett.* **101**, 082405 (2012).
 - [21] H. Liu, C. Zhang, H. Malissa, M. Groesbeck, M. Kavand, R. McLaughlin, S. Jamali, J. Hao, D. Sun, R. A. Davidson, L. Wojcik, J. S. Miller, C. Boehme, and Z. V. Vardeny, Organic-based magnon spintronics, *Nat. Mater.* **17**, 308 (2018).
 - [22] M. Chilcote, M. Harberts, B. Fuhrmann, K. Lehmann, Y. Lu, A. Franson, H. Yu, N. Zhu, H. Tang, G. Schmidt, and E. Johnston-Halperin, Spin-wave confinement and coupling in organic-based magnetic nanostructures, *APL Mater.* **7**, 111108 (2019).
 - [23] A. Franson, N. Zhu, S. Kurfman, M. Chilcote, D. R. Candido, K. S. Buchanan, M. E. Flatté, H. X. Tang, and E. Johnston-Halperin, Low-damping ferromagnetic resonance in electron-beam patterned, high-Q vanadium tetracyanoethylene magnon cavities, *APL Mater.* **7**, 121113 (2019).
 - [24] A. G. Gurevich and G. A. Melkov, *Magnetization Oscillations and Waves* (CRC Press, Inc, New York, 1996).
 - [25] C. Du, T. Van der Sar, T. X. Zhou, P. Upadhyaya, F. Casola, H. Zhang, M. C. Onbasli, C. A. Ross, R. L. Walsworth, and Y. Tserkovnyak, Control and local measurement of the spin chemical potential in a magnetic insulator, *Science* **357**, 195 (2017).
 - [26] D. Labanowski, V. P. Bhalla, Q. Guo, C. M. Purser, B. A. McCullian, P. C. Hammel, and S. Salahuddin, Voltage-driven, local, and efficient excitation of nitrogen-vacancy centers in diamond, *Sci. Adv.* **4**, eaat6574 (2018).
 - [27] M. R. Page, B. A. McCullian, C. M. Purser, J. G. Schulze, T. M. Nakatani, C. S. Wolfe, J. R. Childress, M. E. McConney, B. M. Howe, P. C. Hammel, and V. P. Bhalla, Optically detected ferromagnetic resonance in diverse ferromagnets via nitrogen vacancy centers in diamond, *J. Appl. Phys.* **126**, 124902 (2019).
 - [28] T. van der Sar, F. Casola, R. Walsworth, and A. Yacoby, Nanometre-scale probing of spin waves using single-electron spins, *Nat. Commun.* **6**, 7886 (2015).
 - [29] C. S. Wolfe, V. P. Bhalla, H. L. Wang, C. H. Du, S. Manuilov, R. M. Teeling-Smith, A. J. Berger, R. Adur, F. Y. Yang, and P. C. Hammel, Off-resonant manipulation of spins in diamond via precessing magnetization of a proximal ferromagnet, *Phys. Rev. B* **89**, 180406(R) (2014).
 - [30] C. S. Wolfe, S. A. Manuilov, C. M. Purser, R. Teeling-Smith, C. Dubs, P. C. Hammel, and V. P. Bhalla, Spatially resolved detection of complex ferromagnetic dynamics using optically detected nitrogen-vacancy spins, *Appl. Phys. Lett.* **108**, 232409 (2016).
 - [31] P. Andrich, C. F. de las Casas, X. Liu, H. L. Bretscher, J. R. Berman, F. J. Heremans, P. F. Nealey, and D. D. Awschalom, Long-range Spin wave mediated control of defect qubits in nanodiamonds, *npj Quantum Inf.* **3**, 28 (2017).

- [32] D. Kikuchi, D. Prananto, K. Hayashi, A. Laraoui, N. Mizuochi, M. Hatano, E. Saitoh, Y. Kim, C. A. Meriles, and T. An, Long-distance excitation of nitrogen-vacancy centers in diamond via surface spin waves, *Appl. Phys. Express* **10**, 103004 (2017).
- [33] J. F. Ziegler, M. D. Ziegler, and J. P. Biersack, Srim – The stopping and range of ions in matter (2010), *Nucl. Instrum. Meth. Phys. Res. Sec. B* **268**, 1818 (2010).
- [34] M. Harberts, Y. Lu, H. Yu, A. J. Epstein, and E. Johnston-Halperin, Chemical vapor deposition of an organic magnet, vanadium tetracyanoethylene, *J. Visualized Exp.*, 52891 (2015).
- [35] I. H. Froning, M. Harberts, Y. Lu, H. Yu, A. J. Epstein, and E. Johnston-Halperin, Thin-film encapsulation of the air-sensitive organic-based ferrimagnet vanadium tetracyanoethylene, *Appl. Phys. Lett.* **106**, 122403 (2015).
- [36] M. Harder, Y. Gui, and C.-M. Hu, Electrical detection of magnetization dynamics via spin rectification effects, *Phys. Rep.* **661**, 1 (2016).
- [37] J. P. Tetienne, L. Rondin, P. Spinicelli, M. Chipaux, T. Debuisschert, J. F. Roch, and V. Jacques, Magnetic-field-dependent photodynamics of single NV defects in diamond: An application to qualitative all-optical magnetic imaging, *New J. Phys.* **14**, 103033 (2012).
- [38] C. Kittel, On the theory of ferromagnetic resonance absorption, *Phys. Rev.* **73**, 155 (1948).
- [39] H. Yu, M. Harberts, R. Adur, Y. Lu, P. C. Hammel, E. Johnston-Halperin, and A. J. Epstein, Ultra-narrow ferromagnetic resonance in organic-based thin films grown via low temperature chemical vapor deposition, *Appl. Phys. Lett.* **105**, 012407 (2014).
- [40] C. M. Purser, V. P. Bhalla, F. Guo, M. R. Page, Q. Guo, G. D. Fuchs, and P. C. Hammel, Spinwave detection by nitrogen-vacancy centers in diamond as a function of probe–sample separation, *Appl. Phys. Lett.* **116**, 202401 (2020).
- [41] E. Lee-Wong, R. Xue, F. Ye, A. Kreisel, T. van der Sar, A. Yacoby, and C. R. Du, Nanoscale detection of magnon excitations with variable wavevectors through a quantum spin sensor, *Nano Lett.* **20**, 3284 (2020).
- [42] F. Yang and P. C. Hammel, FMR-driven spin pumping in $\text{Y}_3\text{Fe}_5\text{O}_{12}$ -based structures, *J. Phys. D: Appl. Phys.* **51**, 253001 (2018).